AGU PUBLICATIONS

JGR

Journal of Geophysical Research: Planets

RESEARCH ARTICLE
10.1002/2015JE004917

Key Points:
- SHARAD results can improve ionospheric compensation of MARSIS sounding data
- Total electron content from both sensors can be merged for long-term studies
- Scattering by refraction in the ionosphere occurs over long periods in some regions

Correspondence to:
B. A. Campbell,
campbellb@si.edu

Citation:
Campbell, B. A., and T. R. Watters (2016), Phase compensation of MARSIS subsurface sounding data and estimation of ionospheric properties: New insights from SHARAD results, *J. Geophys. Res. Planets*, *121*, 180–193, doi:10.1002/2015JE004917.

Received 30 JUL 2015
Accepted 6 JAN 2016
Accepted article online 11 JAN 2016
Published online 22 FEB 2016

Phase compensation of MARSIS subsurface sounding data and estimation of ionospheric properties: New insights from SHARAD results

Bruce A. Campbell[1] **and Thomas R. Watters**[1]

[1]Center for Earth and Planetary Studies, Smithsonian Institution, Washington, District of Columbia, USA

Abstract Subsurface radar sounding observations by the Mars Advanced Radar for Subsurface and Ionospheric Sounding (MARSIS) and Shallow Radar (SHARAD) instruments are affected by ionospheric phase distortions that lead to image blurring and delay offsets. Based on experience with SHARAD image correction, we propose that ionospheric blurring in MARSIS radargrams may be compensated with a model of smoothly varying quadratic phase errors along the track. This method yields well-focused radargrams for geologic interpretation and allows analysis of the validity range for models used to derive total electron content (TEC) from phase distortion terms in previous MARSIS studies. The quadratic term appears to be a good proxy for TEC at solar zenith angles >65° for MARSIS Band 4 (5 MHz) and >75° for Band 3 (4 MHz). Comparison of MARSIS- and SHARAD-derived TEC values from 2007 to 2014 reveals correlations in seasonal behavior and in the characterization of ionospheric activity due to coronal mass ejections. We also present SHARAD and MARSIS evidence for a persistent region of anomalous radar scattering south of Arsia Mons. These echoes have been previously suggested to arise from refraction of the radar signal by electron density variations. There are no strong signatures, however, in the quadratic image compensation term correlated with the anomalous scattering, suggesting either that electron density variations responsible for refracted signal paths occur primarily in regions offset from the spacecraft track or that these density changes have a minimal impact on the integrated phase distortion of the subspacecraft footprint. We suggest observations and analyses to better constrain the mechanism and timing of such echoes.

1. Introduction

The ionosphere of Mars exhibits fluctuations in electron content with time and geographic location due to variations in distance from the Sun, the degree of solar activity, local solar zenith angle, and remnant crustal magnetic fields. Electron density varies with altitude above the surface, with a scale height between 8 and 30 km and a maximum dayside density at altitudes from about 120 to 150 km [*Gurnett et al.*, 2005; *Withers et al.*, 2012]. The spatial and temporal characteristics of the electron density are of interest as a measure of ionospheric activity [e.g., *Withers*, 2009], and because of their impact on radar-sounding observations of the surface and subsurface. This work examines current methods for correcting ionospheric effects in orbital radar sounding data, demonstrates a new approach based on recent studies of spatial variation in the electron density, and discusses implications for estimating the total electron content (TEC) and understanding anomalous features in the sounder data.

Two radar-sounding instruments are currently in orbit at Mars. The Mars Express spacecraft carries the Mars Advanced Radar for Subsurface and Ionospheric Sounding (MARSIS) [*Picardi et al.*, 2005; *Jordan et al.*, 2009], while the Mars Reconnaissance Orbiter carries the Shallow Radar (SHARAD) instrument [*Seu et al.*, 2007]. MARSIS subsurface sounding observations utilize one of four bands with center frequencies, f_0, of 5 MHz, 4 MHz, 3 MHz, and 1.8 MHz. The bandwidth of the linear frequency-modulated "chirp" signal is 1 MHz for each mode. SHARAD operates at a single center frequency of 20 MHz, with a 10 MHz chirp bandwidth. The resulting free-space, one-way vertical resolution is 150 m for MARSIS and 15 m for SHARAD, reduced by the root of the real permittivity, ε', for propagation in geologic materials (about 80 m and 8 m, respectively, in water ice, for which ε' is about 3.2).

Because the transmitted power is low, the chirp signal allows for recovery of fine time resolution from a pulse that is 250 μs long for MARSIS and 85 μs long for SHARAD. The reflected signal is correlated with a model for the original swept-frequency chirp to achieve a much shorter effective pulse ("range compression"), but the ionosphere can complicate this process. A radar signal passing through the ionosphere experiences three

effects: (1) an increased time delay with respect to that determined from the speed of light in vacuum, (2) distortion of the range-compressed echo due to variations in phase over the frequency range of the chirp, and (3) attenuation of the reflected signal. The impact of the ionosphere increases for lower frequency radar, and if the signal approaches the plasma frequency, there is essentially no propagation.

The desire to obtain subsurface sounding data means that many observations from both instruments must be corrected for the delay and distortion effects—there is no way to recover power lost due to attenuation. MARSIS began operations in July 2005, and several approaches to ionosphere compensation and TEC estimation are well documented [*Safaeinili et al.*, 2003, 2007; *Mouginot et al.*, 2008; *Zhang et al.*, 2009; *Cartacci et al.*, 2013]. These studies show that MARSIS observations are affected by the ionosphere to a solar zenith angle (SZA) value of about 120°, rather far onto the "nightside" of Mars. MARSIS also has an active topside sounding mode (AIS), used to characterize the upper layers of the ionosphere, and assess the impact of crustal magnetic fields [*Gurnett et al.*, 2005; *Duru et al.*, 2006]. SHARAD arrived at Mars in 2006, and subsequent work has addressed the smaller but still important effects of the ionosphere [*Campbell et al.*, 2011, 2014]. SHARAD echoes, due to their higher frequency, are little impacted beyond SZA values of about 100°.

Recent experience with SHARAD data sheds new light on how the ionosphere of Mars behaves over relatively short (few tens of kilometers) length scales, and the large number of orbit crossovers at different solar zenith angles, and thus echo delay, allows for well-calibrated estimates of the total electron content. Taken together, these findings motivate a new look at the correction of MARSIS data for ionospheric blurring effects, and at the retrieval of TEC values from these observations. We first provide a synopsis of how the electron density affects radar signals, and the methods used to date in correcting MARSIS and SHARAD echoes (section 2). We then compare TEC estimates from the two sensors during periods of overlapping observation, use SHARAD data to support a new method for representing the along-track changes in MARSIS phase distortion, and demonstrate the utility of this method to improve recovery of the subsurface sounding information (section 3). In section 4, we revisit the estimation of TEC from MARSIS based on the information extracted from the new compensation scheme. In section 5, we use the extended temporal coverage from the two sounders to study long-lived ionospheric effects south of Arsia Mons. Section 6 summarizes results and directions for future work.

2. Ionospheric Distortion, Compensation, and TEC Estimation

The electron content of a planetary ionosphere may have a complicated distribution as a function of height above the surface, with a peak density that can vary in both amplitude and elevation [e.g., *Withers et al.*, 2012]. Depending on the degree of solar activity, collisional interactions between neutral particles in the atmosphere may also play an important role. Active sounding from high altitude can probe this distribution by obtaining reflections from regions of enhanced electron content [e.g., *Gurnett et al.*, 2005; *Duru et al.*, 2006]. Signals from an orbiting subsurface sounder, in contrast, traverse the lower ionosphere, ideally without undergoing such reflections. The primary goal of ionospheric compensation is thus to obtain a high-quality radargram for geologic studies, with a secondary goal of retrieving information on the electron content.

The radargrams, two-dimensional representations of echo power with along-track location and signal time delay, for MARSIS and SHARAD are built up from a series of individual "frames," each of which represents a certain number of echo records received in response to transmitted pulses. These batches of echoes are Doppler processed to narrow the along-track resolution and improve the signal-to-noise performance through coherent summation of signals from a given point of the surface or subsurface as it passes beneath the sensor [e.g., *Picardi et al.*, 2004; *Seu et al.*, 2007]. Figure 1 shows representative MARSIS and SHARAD radargrams over the south polar layered deposits of Mars, highlighting the differences in depth of penetration and vertical/horizontal spatial resolution. Our main concern here is with the range compression of signals, rather than the choice of parameters for Doppler processing. In this section, we review the basic effects of the electron density on a linear frequency-modulated (chirp) radar signal, and the methods currently used to correct MARSIS and SHARAD data.

2.1. Phase Effects on a Radar Signal

MARSIS and SHARAD signals can be approximated by a linear frequency ramp over the duration of the chirp. In reality, the transmitted signal has variations in amplitude (and perhaps phase) due to the imperfect impedance

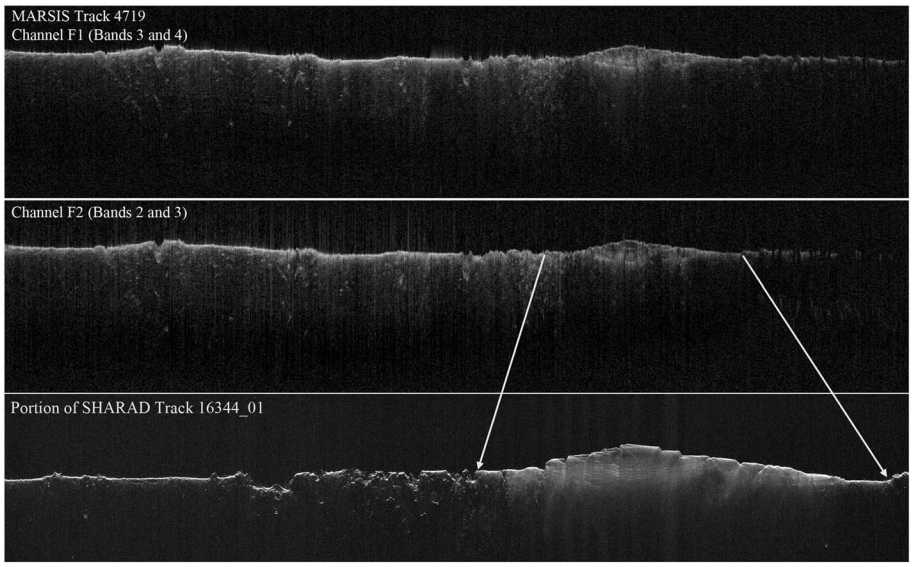

Figure 1. Radargrams for both channels (F1 and F2) of MARSIS track 4719, processed using the autofocus algorithm discussed in this paper. The south polar layered deposits (SPLD) of Mars are at right. Bottom panel is portion of nearby SHARAD track 16344_01, showing the SPLD layering in more detail, but with almost no reflection from the bright basal reflector seen by MARSIS. Arrows denote approximately correlated locations in the two data sets.

match between the signal and the dipole antenna and matching network, but neglecting these aspects appears to still allow stable ionospheric modeling results [e.g., *Campbell et al.*, 2014]. The MARSIS "up-swept" chirp can be expressed as an instantaneous angular frequency, φ, that varies with time, t, from the start of the pulse:

$$\varphi(t) = 2\pi(F_L + at) \tag{1}$$

where F_L is the low-frequency end of the signal bandwidth and a is the chirp rate (in Hz/s). The actual phase function, Φ, applied to the transmitted signal is the integral of $\varphi(t)$ over time, so the basic form is quadratic:

$$\Phi(t) = 2\pi\left(tF_L + \frac{a}{2}t^2\right) \tag{2}$$

and the discrete, complex values of the chirp compression function are the following:

$$C_i = -sin(\Phi(t_i)) + icos(\Phi(t_i)) \tag{3}$$

For MARSIS, t_i is incremented by about 0.714 μs for each of 490 complex samples (a 1.4 MHz sampling rate) and a is 4.0×10^9 Hz/s. For SHARAD the time increment between the 3600 real-valued samples is 0.0375 μs, and a is about 7.4×10^{10} Hz/s. In the absence of ionospheric effects, echoes collected by the receiver can be range compressed to power format by multiplying the frequency domain signal spectrum by the conjugate of the Fourier transform of the chirp phase function (equation (3)), performing an inverse Fourier transform, and taking the squared magnitude of the complex signal.

The ionosphere distorts the phase of the radar signal as it transits the column of electrons, with a dependence on frequency that leads to degradation of the range-compressed surface and subsurface echoes. Mitigating this distortion in the range compression requires an additional function that modifies either the reflected signals or the reference chirp. The most common approach to date expresses the necessary correction function in terms of the constituent frequencies of the chirp and the physical parameters of the ionosphere, primarily the electron density as a function of altitude, z, above the surface, $N(z)$. Expansion of this function and retention of only terms up to third order leads to an approximation in inverse powers of the radar frequency, f, and the moments of the electron density distribution [*Safaeinili et al.*, 2007]:

$$\Delta\varphi(f) = \frac{-2\pi}{c}\left[\frac{8.98^2}{f}\int N(z)\mathrm{d}z + \frac{8.98^4}{3f^3}\int N^2(z)\mathrm{d}z + \frac{8.98^6}{8f^5}\int N^3(z)\mathrm{d}z\right] \tag{4}$$

The first integral is the total electron content, in number per square meter, often normalized by a factor of 10^{-16} to "TEC units" or TECUs. A realistic model of the phase distortion requires a description of the ionosphere that typically includes a scale height, maximum electron density, and overall shape with altitude (e.g., Gaussian, quadratic, and triangular). Equation (4) allows for a description of the distortion based on three parameters (a_1, a_2, and a_3) related to the moments of the electron distribution [*Safaeinili et al*., 2007; *Mouginot et al*., 2008; *Cartacci et al*., 2013]. *Zhang et al*. [2009] propose an extension of this function to include effects due to collisional interactions in the neutral atmosphere, thus adding additional terms.

We can also represent the phase variation without reference to any particular physical model for how it is generated in the ionosphere. In this view, the chirp is distorted as function of time along the pulse, and the correction process is the derivation of an optimum "matched filter" for range compression. Starting from equation (2), the distorted chirp is given, to third order, by

$$\Phi(t) = \pi\left[2t(F_L + \alpha) + t^2(a + \beta) + t^3\chi\right] \tag{5}$$

Here α represents a linear term that leads only to a delay (i.e., vertical position) offset in the radargram frames, and β and χ define the quadratic and cubic errors that cause image distortion. Higher-order distortions are not expected to play a significant role in the sounder echoes, and even the cubic term may be negligible if the sounder's operating band is properly chosen to be well above the plasma frequency. The α term is similar to the a_1 term in common applications of equation (4), while the a_2 and a_3 terms of those expansions may mix the quadratic and cubic phase components to some degree [*Cartacci et al*., 2013].

Schemes for mitigating phase distortion in the range compression, using either of the models above, can be described as autofocusing—using the echoes themselves as the metric for the compensation algorithm and optimizing the strength (signal-to-noise ratio, or SNR) of the reflected power. This approach has been proven successful in imaging radar applications, using a variety of functional representations for the phase errors and for the search algorithms that optimize the final product. One important note is that autofocus algorithms generally rely on a degree of redundancy, such as multiple bright scattering features in a scene, to yield a "true" maximum signal response in the presence of clutter and noise [e.g., *Wahl et al*., 1994; *Fienup and Miller*, 2003].

2.2. MARSIS Processing

MARSIS data in the most frequently used subsurface mode (SS3) are processed on the spacecraft to create spectra for three Doppler filters (a trailing frequency bin, a center or nadir bin, and a leading frequency bin), and these spectra are transmitted to the ground without being range compressed [*Jordan et al*., 2009]. The spectra are converted to baseband, so $F_L = -0.5$ MHz (equation (1)) for all operating bands. Each SS3 record contains two channels, termed F1 and F2, with echoes in frequencies selected from the four possible based on the solar zenith angle, and thus often switching as the SZA changes along track. Considerable work has been done in relating the MARSIS range compression to estimates of ionospheric properties while optimizing the signal-to-noise ratio of the radargrams.

Safaeinili et al. [2007] use the formulation of equation (4), optimizing the a_n terms by reference to the time delay between the sensor and the surface at the elevation defined by the Mars Orbital Laser Altimeter (MOLA), and to a maximum SNR of echoes within each frame. *Mouginot et al*. [2008] use a Gaussian model for the electron density profile, and seed each succeeding optimization with the parameters defined from the previous frame. Both frequency channels of the SS3 mode, F1 and F2, are optimized simultaneously on the assumption that the chosen ionosphere structure model, which constrains relationships between the a_n terms, is appropriate over the range of the MARSIS bands (1.3 MHz to 5.5 MHz). The a_1 value (the coefficient on the first-order term of equation (4)) derived from this technique is used to form the Planetary Data System (PDS) archive of MARSIS TEC estimates. *Zhang et al*. [2009] propose a more complex physical ionosphere model that includes neutral collision effects. Finally, *Cartacci et al*. [2013] present a study of nightside MARSIS tracks, treating the F1 and F2 channels independently and deriving a TEC estimate based on the a_2 term and the center frequency, f_0, of the MARSIS band:

$$\mathrm{TEC} = \frac{a_2 c f_0^3}{2\pi(8.98)^2} \tag{6}$$

The results of *Safaeinili et al*. [2007] and *Cartacci et al*. [2013] demonstrate possible correlations between the component of the remnant crustal magnetic field perpendicular to the surface and the electron content of the ionosphere.

As a general observation, the TEC values derived by these methods have significant variability within groups of frames, and occasional anomalous spikes. The quality of the radargrams is also affected, since the autofocus method has not converged in these frames to the true distortion function. The range of variation, as a fraction of the mean TEC value, appears to be larger at smaller values of the SZA. We suggest that much of this behavior stems from application of autofocus techniques to a single echo record, in the presence of noise, rather than to the groups of observations typical of many SAR focusing studies. There are also questions about the magnitude of derived TEC values, which are high relative to the AIS measurements under dayside conditions [*Sanchez-Cano et al*., 2015].

As both *Cartacci et al*. [2013] and *Sanchez-Cano et al*. [2015] note, application of equation (6) is based on assumptions that may break down at higher electron densities. *Cartacci et al*. [2013] suggest that their TEC values are systematically overestimated, with the error increasing to 10% or more at the lowest solar zenith angles. They thus limit their study of possible magnetic field effects to SZA $> 90°$. The impact of model approximations on the TEC results of *Mouginot et al*. [2008], using the a_1 term, is uncertain. Results from SHARAD suggest that a modified approach to MARSIS processing (section 3) can yield improvements in radargram image recovery, shed light on where these earlier methods of TEC estimation can yield robust results, and provide a stable solution for examination of long-term trends in ionospheric behavior.

2.3. SHARAD Processing

SHARAD data offer an advantage in understanding the nature of ionospheric distortion due to their higher sampling rate relative to the ground speed of the spacecraft and the capability to downlink the full record of all pulses without onboard processing. The compensation for products delivered by the U.S. instrument team to the PDS is based on autofocusing, with the "downswept" linear chirp modified by an empirically derived function given by

$$\Phi(t) = E[F_H - at]^{-1.93} \tag{7}$$

where F_H is the maximum chirp frequency (25 MHz) and E is a scalar parameter optimized by the autofocusing. The fixed power law exponent means that the coefficients of the quadratic (β) and cubic (χ) phase distortion terms have a fixed ratio [*Campbell et al*., 2011], and this approximation appears valid over the SHARAD frequency band. For groups of observations, typically spanning about 35 km along the track, the autofocus method optimizes the SNR, and the derived compensation is applied to all radargram frames within the region. The scalar coefficient, E, has a close correlation with delay offsets at hundreds of orbit crossover locations observed at different solar zenith angles, showing that a very good approximation for the TEC is $0.29E$ [*Campbell et al*., 2014]. This "calibration" of the TEC values is accurate enough to reduce the RMS errors in surface echo vertical positioning to just a few range cells (i.e., <50 m).

SHARAD results suggest a generally smooth, cosine-like drop in TEC with solar zenith angle, as predicted by the model of *Chapman* [1931], with broad fluctuations of 10–20% due to localized nightside effects possibly linked with remnant crustal magnetic fields [*Campbell et al*., 2011] and dayside conditions modulated by these fields and other mechanisms [*Withers*, 2009]. In thousands of SHARAD tracks processed to date, we also observe that changes in the total electron content of the ionosphere are smooth down to the scale of the radargram postings (about 500 m). If there were poorly modeled spatial-frequency (few kilometers to 500 m) shifts in the phase distortion, we would expect to see badly range-compressed areas within each 35 km region.

2.4. Comparing MARSIS and SHARAD Data

We can illustrate the similarities and differences in sounder estimates of the TEC during a period of overlap, December 2006 to September 2007, between the PDS-released MARSIS products (Tracks 3748–4808) based on the method of *Mouginot et al*. [2008] and the PDS archive of SHARAD observations (Tracks 1689–5522) based on *Campbell et al*. [2011, 2014]. Figure 2 shows the average and standard deviation of the TEC derived from both data sets during this period. It is clear that MARSIS values tend to exceed those from SHARAD, and the maximum offset between them is about 10%. The standard deviation of the MARSIS estimates rises

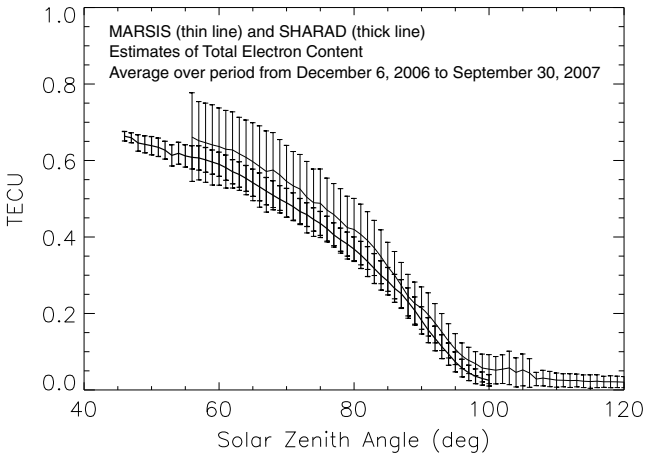

Figure 2. Comparison of total electron content unit estimates for the period from 6 December 2006 to 30 September 2007 from MARSIS [*Mouginot et al*., 2008] and SHARAD [*Campbell et al*., 2011, 2013] data. Note that MARSIS TECU estimates exceed those from SHARAD by up to about 10% and exhibit progressively greater variance with smaller solar zenith angle.

steadily onto the dayside, whereas the higher SHARAD frequency and greater degree of redundancy for autofocusing allow a more consistent TEC estimation performance to SZA values as low as 45°. The typical outcome of the two approaches is shown by tracks obtained just a day apart in 2007 (Figure 3); again, the MARSIS estimates become progressively more widely scattered and larger than the SHARAD values at smaller SZA.

3. A New Approach to MARSIS Ionosphere Compensation

Earlier efforts to compensate ionospheric effects on the MARSIS echoes assume that the phase distortion varies significantly between successive frame acquisitions and thus that the autofocusing must operate on a single frame at a time. While the phase effects likely do vary rapidly, SHARAD results (section 2) support the notion that these changes can be well modeled by smooth functions of the along-track location, as expressed here by the frame number within each segment of the track defined by the use of one of the operating frequency bands. We thus represent the quadratic phase term in equation (5), β, by a polynomial function of this along-track frame number, n, over each period of a chosen frequency in the F1 and F2 channels. The two channels are optimized independently as are the individual segments. We do not index the polynomial to solar zenith angle because for MARSIS polar observations the same SZA value can occur at two locations along the track. The choice of equation (5) to represent the distortion distances our approach from any physical description of the electron density distribution, but it does provide significant insight into limits on assumptions about the linkage of quadratic errors and TEC as a function of solar zenith angle.

For each single-band segment of the F1 and F2 radargrams, we optimize the quadratic error term by reference to the summed SNR of all constituent frames in the segment. A seventh-order polynomial on the frame number appears to adequately represent the along-track fluctuations in β:

$$\beta(n) = \sum_{i=0}^{7} C_i n^i \qquad (8)$$

with the coefficients, C_i, optimized through a downhill simplex minimization algorithm (IDL's AMOEBA) using the summed SNR as a metric. The great value here is that the autofocusing can exploit the redundancy in groups of frames to achieve a robust solution to the range compression. Figure 4 shows how the fitting yields a piecewise solution for the ionospheric behavior along a MARSIS track. As with most other methods, we sum the signals from all three Doppler channels to reduce speckle in the radargram, though this may reduce the SNR of extremely smooth surfaces to some degree (i.e., by adding

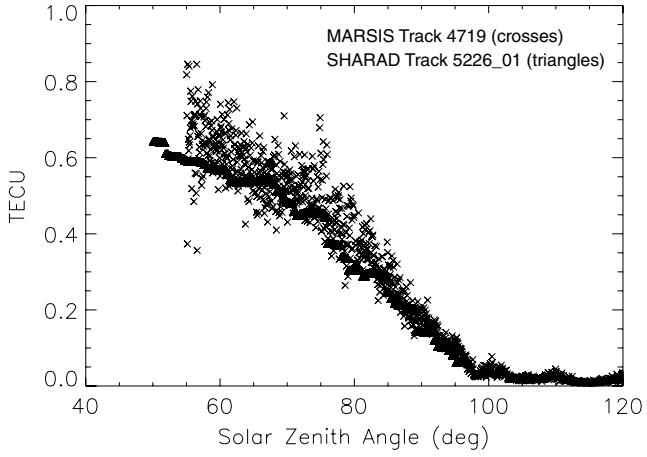

Figure 3. Comparison of estimated total electron content unit values for a MARSIS track collected 6 September 2007 and a SHARAD track collected 7 September 2007. Note that MARSIS values are typically higher than those of SHARAD and exhibit far more variance at solar zenith angles less than about 85°.

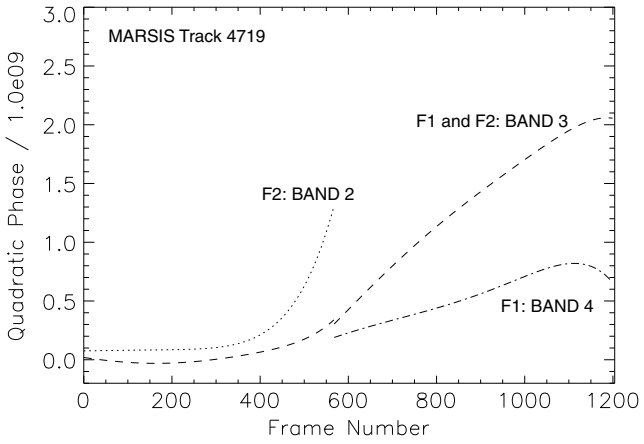

Figure 4. Plot of quadratic phase error term, β, from autofocus solution for both channels, F1 and F2, of MARSIS SS3-Mode Track 4719 (Figure 1). Note that the solutions for Band 3 are nearly continuous across the change in operation.

off-nadir measurements containing little of the specular echo).

A MARSIS SS3 observation may have data from as few as two bands (one each in the F1 and F2 channels) or employ up to all four bands if the range of SZA is large enough to cover both nightside and dayside conditions. Our optimization yields an estimate of the total quadratic phase term, so β is obtained by subtracting the "ideal" 4.0×10^9 Hz/s chirp rate from the component in each frame. Each frame is normalized to the background noise, based on the lowest echo in batches of 32 averaged range cells. With the image distortion corrected, we compensate for variations in the vertical position of the frames by assigning the MOLA elevation to the earliest echo that meets a specified threshold, which changes with the peak SNR to allow for robust selection when the sidelobes of the surface reflection rise above the noise. In general, the optimization process yields good range compression over the length of the radargram (Figure 5). Poor image quality is associated with some of the lowest frequency (Band 1) data, which may overlap with the plasma frequency of the ionosphere, and with frames where the time delay between the pulse transmission and the start of the data recording window (i.e., the range to the surface) was estimated incorrectly.

4. TEC Estimation

Under certain assumptions about ionospheric properties, equation (6) suggests a linear relationship between the quadratic image distortion term and the TEC [*Cartacci et al*., 2013]. A similar assumption appears to hold for the SHARAD data over a wide range of SZA [*Campbell et al*., 2013], but at the lower MARSIS frequencies, there are likely limits on its validity. *Cartacci et al*. [2013] note mismatches between values for the TEC estimated from equation (6) with the different MARSIS bands on the dayside and thus limit their analysis to nightside observations (SZA $>$ 90°). We can use the results of the new autofocus method to examine these behaviors in more detail.

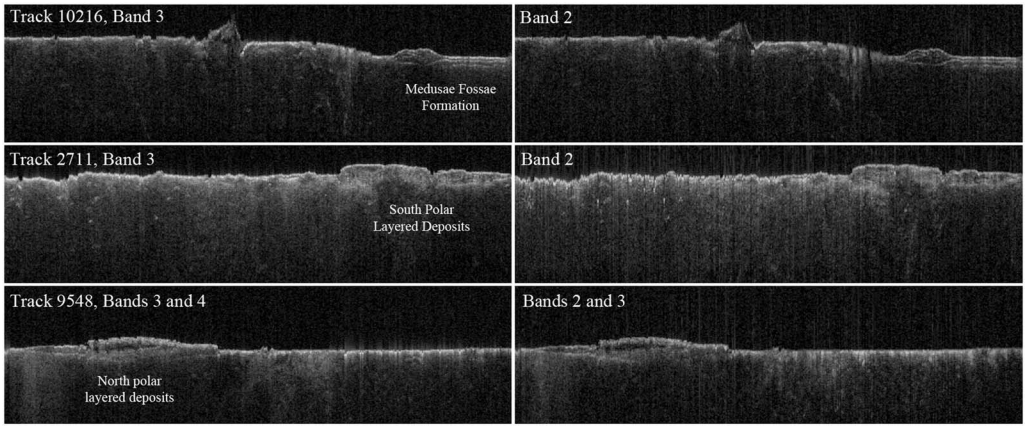

Figure 5. Representative MARSIS tracks showing value of ionospheric correction and registration to MOLA datum for subsurface feature interpretation. Three major landforms are illustrated: the Medusae Fossae Formation and the north and south polar layered deposits. Image width of each panel is 460 MARSIS frames (about 2600 km), and the vertical scale is 178.5 μs.

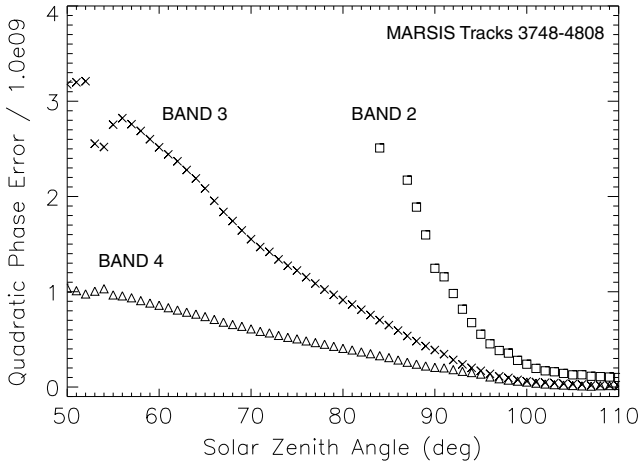

Figure 6. Average quadratic phase error derived from the autofocusing method presented in this paper, plotted as averages in each of three MARSIS bands for tracks 3748–4808, versus solar zenith angle.

Figure 6 shows the average quadratic phase error in MARSIS bands 2–4 (center frequencies of 3.0, 4.0, and 5.0 MHz) for the same group of orbit tracks used in Figure 2 (3748–4808). The angular coverage of Band 2 is much smaller, as dayside ionospheric effects are expected to greatly impact this frequency range. As a tool for understanding the TEC, equation (6) is based on the assumption that the dominant component in the expansion of equation (4) is the $1/f$ term, which is modulated only by the first moment of the electron distribution. If this is the case, then the quadratic phase values should be related as the cube of the ratio of their center frequencies. Applying this scaling to the quadratic phase errors determined from the new method shows an excellent correlation for solar zenith angle values greater than about 75° (Figure 7). This supports a similar conclusion about the range of TEC validity by *Sanchez-Cano et al*. [2015] based on comparisons of estimates from the various subsurface-mode methods with the AIS data.

A comparison of the corrected quadratic terms to the SHARAD TECU estimates for the two tracks used in Figure 3 shows a reasonable match for SZA = 65–75° when the MARSIS β values, after normalization to a 5 MHz frequency, are multiplied by an ad hoc factor of 0.85 (Figure 8). As expected, the agreement between MARSIS and SHARAD TECU estimates occurs over the largest range of SZA for the 5 MHz (Band 4) data, down to about 65°. The new method may thus allow for accurate recovery of the TEC somewhat farther into the dayside than in recent studies, but estimates for SZA less than 65° (Band 4) to 75° (Band 3) will depend upon analyses that might use the frequency dependence in the quadratic phase (equation (4)) to model the higher-order moments of the electron density distribution.

We processed MARSIS tracks from the start of the mission to mid-2014 and compared the resulting TEC estimates to those of SHARAD over the period beginning in early 2007. We used only MARSIS Band 3 data for this test, since it is frequently employed in the SZA range of 75–85°. For every MARSIS or SHARAD track during the time period, we extracted all TECU estimates within this angular range, normalized by cos(SZA) to reduce Chapman-like variations, and averaged the resulting values. Figure 9 shows the two data sets with an arbitrary offset for clarity. Despite gaps in temporal coverage, both TEC estimation methods appear to follow the expected variation with heliocentric longitude, reaching a "local minimum" value at each Mars aphelion (northern summer solstice). The short-term, interorbit variance in TECU values is similar for results from the two sensors.

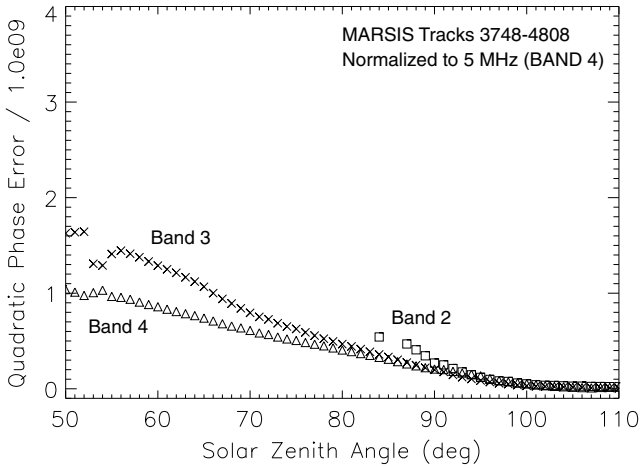

Figure 7. Plot of quadratic phase errors presented in Figure 6, with a scaling factor related to the cube of the MARSIS band center frequency applied to the Band 3 and Band 2 data. The region of overlap from about a solar zenith angle of 75° indicates where estimates of ionospheric TEC would also be in close agreement.

Both radar sounders also detect increases in ionospheric activity, such a major event in early- to mid-2011.

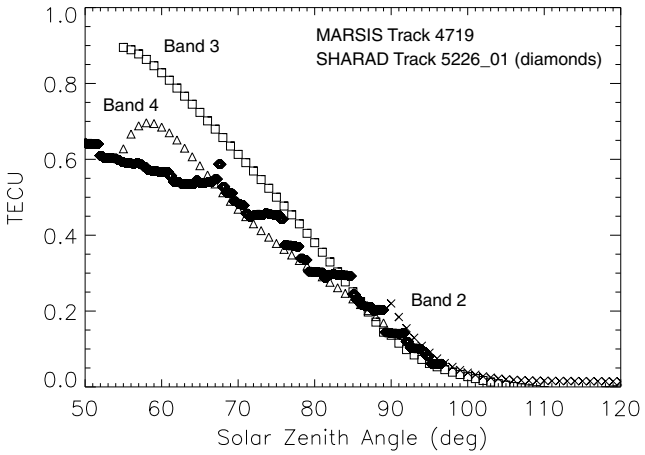

Figure 8. Plot of MARSIS quadratic phase term, β, normalized to 5 MHz frequency, and multiplied by an ad hoc value of 0.85, for Bands 2–4 on Track 4719. Diamonds show TECU values derived for SHARAD track 5226_01. Note that the highest-frequency MARSIS band provides a comparable TECU value down to SZA of about 65°, where the lower frequency Band 3 diverges at about SZA = 75°.

The largest upward excursion in the MARSIS TECU values occurs in early 2011, but it appears that only the waning period of this enhancement was captured by SHARAD due to a gap in observations. The plot of relative values of the TECU parameter from MARSIS and SHARAD shows the potential for integrating data from the two sounders to develop a long-term view of the Martian ionosphere.

5. Persistent Ionospheric Scattering Behavior

One unexpected aspect of the interaction between MARSIS signals and the ionosphere is the frequent occurrence of linear, arcuate, wavy, or parabolic radar echoes at round-trip delay times greater than that of the local surface. In some cases the echo patterns resemble those expected of subsurface scattering features, but they may not reappear identically in subsequent MARSIS observations of the same region [*Picardi et al*., 2005; *Watters et al*., 2006]. *White et al*. [2009] point out a number of such anomalous echoes in the Ma'adim Vallis region. They suggest that the off-nadir reflections arise due to refraction of the transmitted signal by passage through regions of varying electron density, with the beam encountering the surface at normal incidence well away from the nadir point beneath the spacecraft. In this scenario, multiple reflections represent multiple signal paths through the electron-density distribution. *Kane* [2012] models one specific type of parabolic echo pattern, suggesting that these features could occur where the subspacecraft electron density is much lower than the regional average.

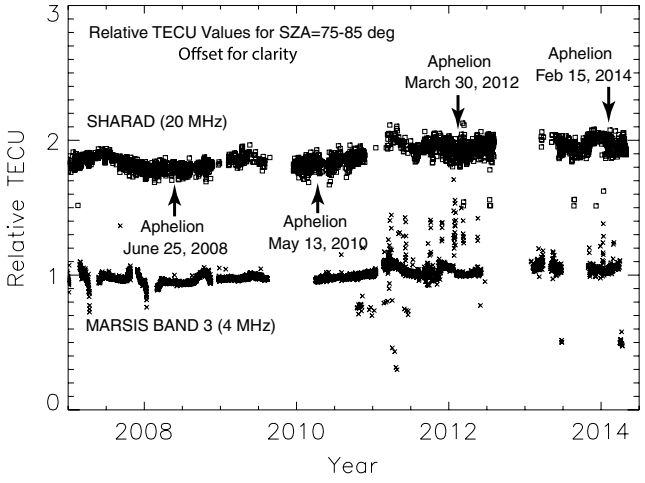

Figure 9. Plot of relative values of the TECU parameter from SHARAD (squares) and MARSIS Band 3 (crosses) data over a time period from early 2007 to mid-2014. The individual plot symbols correspond to one track from the sensor, with values normalized to the cosine of the solar zenith angle and averaged where SZA = 75-85°. The two data sets are offset by an arbitrary value for easier comparison. Arrows denote approximate times of greatest Sun-Mars distance (aphelion).

To date, discussions of these scattering phenomena emphasize their transient nature, though *White et al*. [2009] note several instances near Ma'adim Vallis. The long-term coverage of both radar sounders shows that such features are persistent in a relatively smooth region just south of Arsia Mons, comprising the area from about 13°S to 15°S latitude and about 129°E to 131°E longitude. In at least eight MARSIS tracks from October 2007 to February 2012, there are scattering features that span the range of forms (linear, arcuate, wavy, convex-upward, and convex-downward parabolas) observed elsewhere in "transient" anomalies (Table 1 and Figure 10). Most remarkable is the occurrence on track 6202 of a very clear but quite small, nested-parabola pattern (Figure 11) that mimics those studied by *Watters et al*. [2006] and *Kane* [2012]. There are five tracks in the period from

Table 1. Sounder Observations of the Region South of Arsia Mons[a]

Track	Date	SZA(deg)	MARSISBands	Observations of Ionosphere-Induced Radar Echo Properties
M2778	3/11/2006	109	3, 2	No detection
M3137	6/20/2006	71	4, 3	Strong dayside attenuation
M3908	1/21/2007	111	3, 2	No detection
M4899	10/26/2007	102	3, 2	Wavy reflections
M4910	10/29/2007	101	3, 2	Wavy reflections
M6015	9/7/2008	116	3, 2	Wavy reflections
M6202	10/31/2008	85	4, 3	Nested parabolic pattern
M7084	7/11/2009	93	3, 2	Dual parabolic pattern
M7109	7/18/2009	88	3, 2	Only very weak linear features
S1589701	12/17/2009	47	-	Wavy reflections
M8111	5/3/2010	116	2, 1	Complex, wavy features
M8199	5/28/2010	102	3, 2	No detection
M9130	2/23/2011	112	3, 2	Parabolic pattern
M10339	2/11/2012	91	3, 2	Sharp, narrow parabola
M12248	8/20/2013	112	3, 2	No detection except bright feature near Arsia

[a]MARSIS observations indicated by "M" prefix, and SHARAD observations by "S" prefix. Solar zenith angle (SZA) noted near the center of the anomalous echo region.

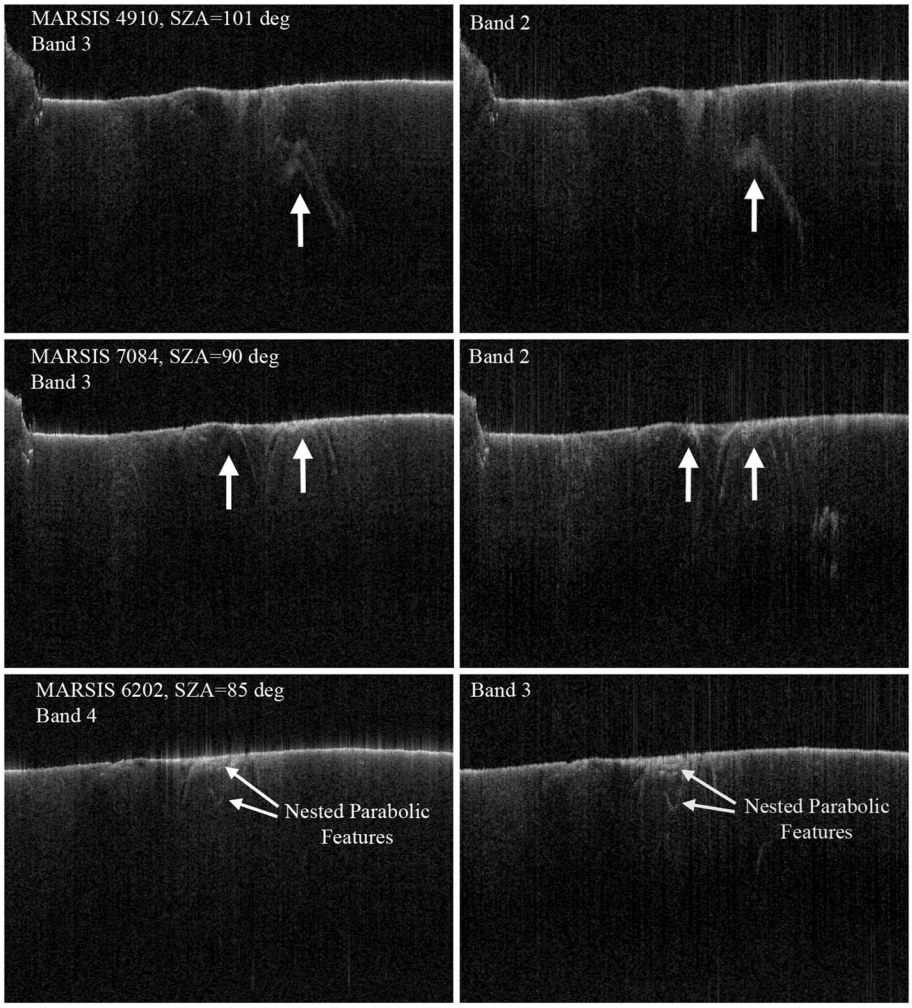

Figure 10. Examples of ionosphere-induced radar scattering features in MARSIS data, highlighted by white arrows, for three tracks over the region south of Arsia Mons (visible at left in the top two tracks). Each panel is about 1700 km in width and represents the full delay range of the MARSIS data. North is to the left in all images.

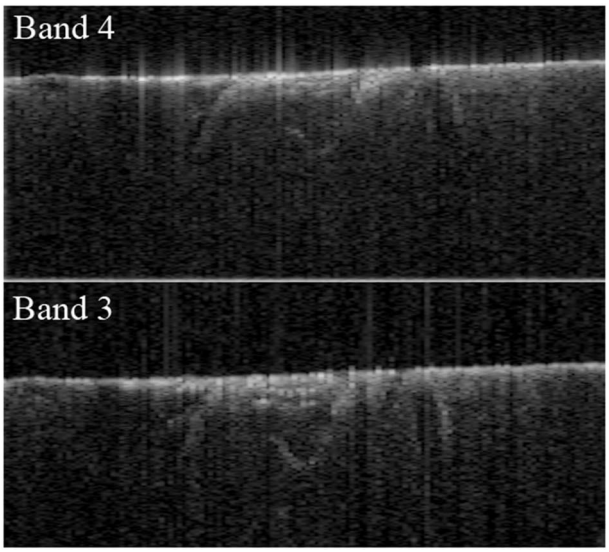

Figure 11. Portion of MARSIS track 6202, with aspect ratio increased two-fold from the images in Figure 10. Image width is about 600 km, and the vertical scale is about 163 μs in round-trip delay time. Note the well-defined nested parabolic echoes, particularly in the Band 3 data.

March 2006 to August 2013 where little or no anomalous behavior is observed. There are also instances, particularly in the lower frequency channel of each SS3 observation, of strong localized echoes that are more irregular in shape. Coverage by SHARAD is much more limited, but on one dayside track (15897_01, 17 December 2009), a wavy echo pattern is clearly observed in the same region (Figure 12). Five other tracks from SHARAD have no evident anomalous scattering.

The long-term presence of these features over a small region of Mars suggests that some mechanism creates distortions of the ionospheric electron density, evidently with different characteristics at different times based on the wide range of echo forms (Figure 10). The MARSIS detections occur for solar zenith angles of 85°–116°, while the nondetections occur for SZA of 88° to 112°. The SHARAD detection occurs well onto the dayside (SZA = 46°–49°), but the derived TECU value of 0.57–0.59 is consistent with the average behavior at this geometry (Figure 2). There is some possibility that the MARSIS detections occur preferentially during periods of higher dayside TEC, but the small sample size does not provide confirmation.

None of the anomalous scattering examples discussed above has a strong associated signature in the quadratic phase distortion term derived from our focusing process. To the extent that these phase errors are related to the total electron content of the column between the sensor and the nadir footprint, we do not see evidence for the "holes" proposed by *Kane* [2012] to explain radar signal refraction. In the magnetic field map derived by *Lillis et al*. [2008], remnant crustal field patterns are detected south of the Tharsis Montes volcanic province, though their magnitude is low relative to features farther south in the highlands. Likewise, the subtle TEC variations relative to a smoothly varying behavior with SZA, noted by *Safaeinili et al*. [2007] and *Cartacci et al*. [2013, Figure 9], do not suggest a unique pattern of behavior south of Arsia Mons.

To provide some insight into how the refraction occurs, and the potential impact on the TEC measured from phase distortion of the nadir-location echo, we examine a model for a "slab" of enhanced electron content that occurs at some altitude and offset from the spacecraft ground track (Figure 13). The edges of this slab or cloud are treated as a rectangular shape—while a natural feature would have a less regular margin, this serves to show the general scattering behavior. The index of refraction, η, of the ionosphere is linked with the electron density, N_e. For units of electrons per cubic centimeter, this relationship is given by [*Andrews et al*., 2013; *Safaeinili et al*., 2007]:

$$\eta = \left[1 - \frac{8980^2 N_e}{f^2}\right]^{1/2} \tag{9}$$

where f is the frequency of the radar signal. Because a plasma has $\eta < 1$, a ray that enters a region of higher electron density bends away from the normal to the interface. The slab vertical edge

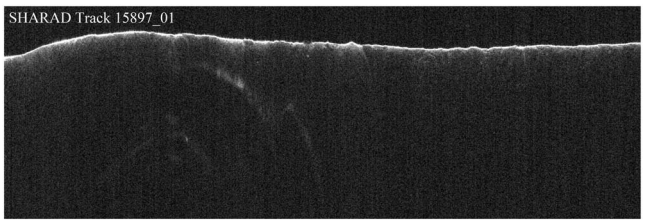

Figure 12. Portion of SHARAD track 15897_01, showing wavy, ionosphere-induced radar scattering features south of Arsia Mons. Image width is about 925 km, and the vertical scale is about 76 μs in round-trip time.

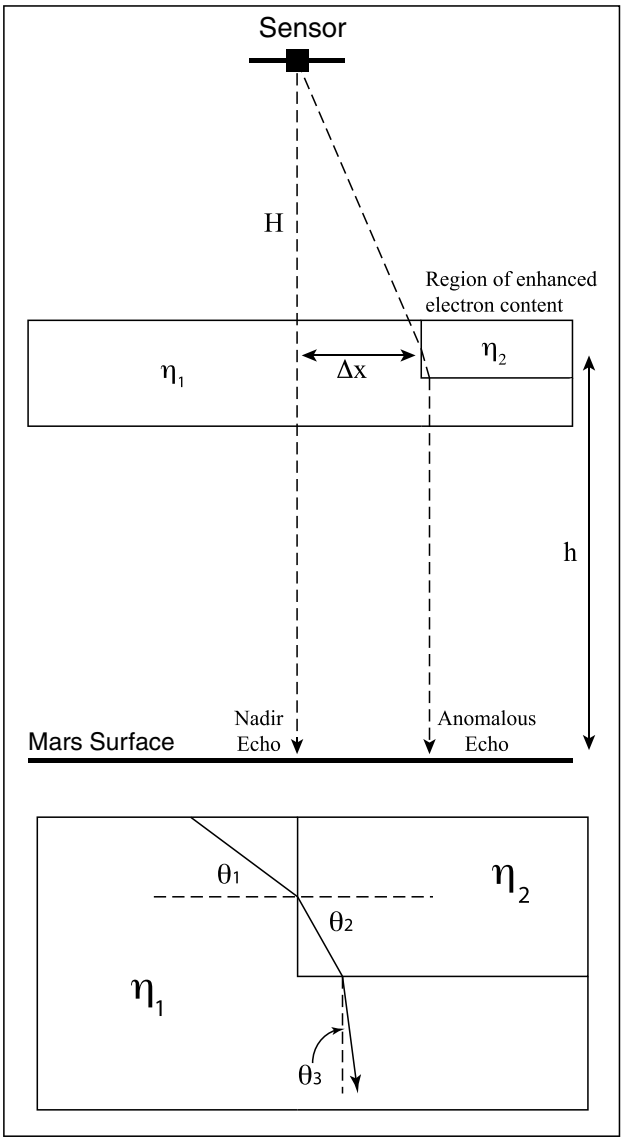

Figure 13. Schematic of radar scattering paths through a slab-like layer of Mars ionosphere. Signals from the sounder reflect from the surface directly below the spacecraft, but refraction due to abrupt interfaces in the electron density can yield additional ray paths that also encounter the surface at normal incidence. Lower diagram shows geometry of refraction in the slab, with labeling of angles discussed in text.

occurs at some altitude, h, and horizontal offset, Δx, from the ground track. We characterize the anomalous MARSIS echoes by their arrival time, Δt, with respect to the nadir surface return, and the spacecraft altitude, H. The slab has a refractive index of η_2, while the subspacecraft region at altitude h is characterized by η_1.

The signal from the sounder reaches the vertical edge of the slab at a local incidence angle of θ_1, which is approximately related to the slab height and offset (neglecting the bending of the ray from the spacecraft by the intervening electrons):

$$\sin\theta_1 = \frac{H-h}{\sqrt{\Delta x^2 + (H-h)^2}} \tag{10}$$

The horizontal offset term is related to the delay offset by

$$\Delta x = \left[\left(H - h + \frac{c\Delta t}{2}\right)^2 - (H-h)^2\right]^{1/2} \tag{11}$$

where we assume that the vertical extent of the slab is too small to affect the travel time of the ray relative to the background ionosphere. Passing into the higher-density plasma, the ray bends toward the surface of Mars, to an angle θ_2 with respect to the normal to the edge of the slab:

$$\sin\theta_2 = \frac{\eta_1}{\eta_2}\sin\theta_1 \tag{12}$$

Finally, the signal enters the background electron content level, bending to an angle θ_3 that is even closer to the normal to the Martian surface. Using small-angle approximations where appropriate:

$$\theta_3 \approx \frac{\eta_2}{\eta_1}\left[1 - \frac{1}{2}\left(\frac{\eta_1}{\eta_2}\sin\theta_1\right)^2\right] \tag{13}$$

Our requirement for encountering the surface at normal incidence means that θ_3 must approach zero, which occurs when

$$\frac{\eta_1}{\eta_2}\sin\theta_1 = \sqrt{2} \tag{14}$$

We can thus define the electron content of the slab based on values for the spacecraft altitude, slab edge location, electron content at the slab altitude along the subspacecraft axis, and the delay offset of the particular MARSIS echo from the surface return. Note that if an anomalous echo is present in a particular MARSIS band, we expect little difference in the time delay offset for echoes at lower frequencies, since the ray is

simply bent more toward the Mars surface normal by the higher refractive-index contrast induced by the change in electron density (equation (9)). At some point, however, lower frequency signals may reach the criterion for total internal reflection and simply bounce off the slab margin.

As an example, consider an anomalous echo that occurs 10 μs (about 14 MARSIS range cells) after the surface return in Band 3 ($f = 4$ MHz) for a spacecraft altitude of 350 km. If the slab occurs at an altitude of 130 km, near the typical peak of the dayside electron density, then the edge of the slab is offset by ~26 km from the spacecraft ground track. If the background density is $1.0 \times 10^5\,\mathrm{cm}^{-3}$ at 130 km altitude beneath the spacecraft, then the slab density must be about 50% higher to produce the necessary refraction path. These geometric and electron density values are consistent with the results of *Kane* [2012], though we have allowed the contrast to occur due to the off-nadir slab rather than a subspacecraft "hole." Our model does not at present, however, capture the azimuthal symmetry in refraction paths required by some of the most complex observed scattering features.

When anomalous echoes occur, how much of a signature should we expect in the TEC value derived from autofocusing of reflections from the nadir region of the ground track? These features may have little discernible impact on a TEC value inferred from the quadratic phase distortion or a comparison of delay time to MOLA data, especially if the enhanced electron content is some distance from the ground track (Figure 13). In addition, the enhancement in electron content need only occur over a small vertical scale to create the refraction, so the effect on the integrated column abundance will depend upon the shape of the full distribution with altitude. A survey of dayside column shape and variability by *Withers et al*. [2012] suggests that thin (kilometer-scale) slabs or clouds of higher electron content might be difficult to discern from the integral over the often complex vertical distribution. It would be interesting to collect subsurface sounding data over short time periods (days to weeks) across substantial (hundreds of kilometers) regions, in order to map the complexity of the TEC signature and perhaps find evidence for persistent spatial patterns. Such experiments are certainly possible with SHARAD.

6. Conclusions

Observations by the MARSIS and SHARAD radar sounders are affected by ionospheric phase distortion for dayside observations, and to varying degrees in the nightside region. Based on experience with total electron content estimation and image correction from SHARAD data, we propose that ionospheric blurring of the MARSIS radargrams may be effectively compensated with a model of smoothly varying quadratic phase errors along the track. This approach allows analysis of the validity range for models used for TEC estimation in previous MARSIS studies. We conclude that a linkage between the quadratic phase distortion term and the TEC can yield robust estimates of the total electron content for solar zenith angles $>65°$ for MARSIS Band 4 and $>75°$ for MARSIS Band 3, consistent with empirical analyses by *Sanchez-Cano et al*. [2015]. The proposed methodology yields well-focused radargrams for geologic interpretation and provides a robust and less locally (i.e., frame to frame) variable solution for the general behavior of the ionosphere along a MARSIS track. Comparison of the derived MARSIS and SHARAD TEC values from 2007 to 2014 reveals good correlation in both seasonal behavior and in the characterization of anomalous ionospheric activity due to coronal mass ejections. Finally, we presented SHARAD and MARSIS evidence for the existence of at least one persistent region of anomalous ionospheric radar scattering and suggested future observations that might better constrain the mechanism, extent, and timing of these features. In particular, it may be worthwhile to collect subsurface sounding data over regions of interest on short enough time scales to map lateral fluctuations in the ionosphere.

Acknowledgments

The authors thank R. Orosei for helpful discussions about MARSIS data formats. Insightful reviews of the manuscript were provided by R. Orosei, T. Kobayashi, W. Fa, and an anonymous referee. The Shallow Subsurface Radar (SHARAD) was provided by the Italian Space Agency (ASI), and its operations are led by the DIET Department, University of Rome "La Sapienza" under an ASI science contract. All SHARAD data used in this work are available through the Geoscience Node of the Planetary Data System (http://pds-geosciences.wustl.edu/missions/mro/sharad.htm). The MARSIS data are, at present, archived with the PDS only through orbit 3068 (http://pds-geosciences.wustl.edu/missions/mars_express/marsis.htm). Our methodology for the radargram focusing and recovery of TEC values may be validated from these available data.

References

Andrews, D. J., H. J. Opgenoorth, N. J. T. Edberg, M. Andre, M. Franz, E. Dubinin, F. Duru, D. Morgan, and O. Witasse (2013), Determination of local plasma densities with the MARSIS radar: Asymmetries in the high-altitude Martian ionosphere, *J. Geophys. Res. Space Physics*, *118*, 6228–6242, doi:10.1002/jgra.50593.

Campbell, B. A., N. E. Putzig, L. M. Carter, and R. J. Phillips (2011), Autofocus correction of phase distortion effects on SHARAD echoes, *IEEE Geosci. Remote Sens. Lett.*, *8*, 939–942, doi:10.1109/LGRS.2011.2143692.

Campbell, B. A., N. E. Putzig, L. M. Carter, G. A. Morgan, R. J. Phillips, and J. J. Plaut (2013), Roughness and near-surface density of Mars from SHARAD radar echoes, *J. Geophys. Res. Planets*, *118*, 436–450, doi:10.1002/jgre.20050.

Campbell, B. A., N. E. Putzig, F. J. Foss II, and R. J. Phillips (2014), SHARAD signal attenuation and delay offsets due to the Martian ionosphere, *IEEE Geosci. Remote Sens. Lett.*, *11*, 632–635, doi:10.1109/LGRS.2013.2273396.

Cartacci, M., E. Amata, A. Cicchetti, R. Noschese, S. Giuppi, B. Langlais, A. Frigeri, R. Orosei, and G. Picardi (2013), Mars ionosphere total electron content analysis from MARSIS subsurface data, *Icarus*, *223*, 423–437, doi:10.1016/j.icarus.2012.12.011.

Chapman, S. (1931), Absorption and dissociative or ionising effects of monochromatic radiation in an atmosphere on a rotating Earth, *Proc. Phys. Soc. London*, *43*, 1047–1055.

Duru, F., D. A. Gurnett, T. F. Averkamp, D. L. Kirchner, R. L. Huff, A. M. Persoon, J. J. Plaut, and G. Picardi (2006), Magnetically controlled structures in the ionosphere of Mars, *J. Geophys. Res.*, *111*, A12204, doi:10.1029/2006JA011975.

Fienup, J. R., and J. J. Miller (2003), Aberration correction by maximizing generalized sharpness metrics, *J. Opt. Soc. Am. A Opt. Image Sci.*, *20*, 609–620.

Gurnett, D. A., et al. (2005), Radar soundings of the ionosphere of Mars, *Science*, *310*, 1929–1933.

Jordan, R., et al. (2009), The Mars Express MARSIS sounder instrument, *Planet. Space Sci.*, *57*, 1975–1986, doi:10.1016/j.pss.2009.09.016.

Kane, M. V. (2012), Transient subsurface features in Mars Express radar data: An explanation based on ionospheric holes, MS thesis, Univ. of Iowa. [Available at http://ir.uiowa.edu/etd/3477.]

Lillis, R. J., H. V. Frey, M. Manga, D. L. Mitchell, R. P. Lin, M. H. Acuna, and S. W. Bougher (2008), An improved crustal magnetic field map of Mars from electron reflectometry: Highland volcano magmatic history and the end of the Martian dynamo, *Icarus*, *194*, 575–596, doi:10.1016/j.icarus.2007.09.032.

Mouginot, J., W. Kofman, A. Safaeinili, and A. Herique (2008), Correction of the ionospheric distortion on the MARSIS surface sounding echoes, *Planet. Space Sci.*, *56*, 917–926, doi:10.1016/j.pss.2008.01.010.

Picardi, G., et al. (2004), Performance and surface scattering models for the Mars Advanced Radar for Subsurface and Ionosphere Sounding (MARSIS), *Planet. Space Sci.*, *52*, 149–156, doi:10.1016/j.pss.2003.08.020.

Picardi, G., et al. (2005), Radar soundings of the subsurface of Mars, *Science*, *310*, 1925–1928.

Safaeinili, A., W. Kofman, J. Nouvel, A. Herique, and R. L. Jordan (2003), Impact of Mars ionosphere on orbital radar sounder operation and data processing, *Planet. Space Sci.*, *51*, 505–515.

Safaeinili, A., W. Kofman, J. Mouginot, Y. Gim, A. Herique, A. B. Ivanov, J. J. Plaut, and G. Picardi (2007), Estimation of the total electron content of the Martian ionosphere using radar sounder surface echoes, *Geophys. Res. Lett.*, *34*, L23204, doi:10.1029/2007GL032154.

Sanchez-Cano, B., et al. (2015), Total electron content in the Martian atmosphere: A critical assessment of the Mars Express MARSIS data sets, *J. Geophys. Res. Space Physics*, *120*, 2166–2182, doi:10.1002/2014JA020630.

Seu, R., et al. (2007), The SHARAD sounding radar on MRO, *J. Geophys. Res.*, *112*, E05S05, doi:10.1029/2006JE002745.

Wahl, D. E., P. H. Eichel, D. C. Ghiglia, and C. V. Jakowatz (1994), Phase gradient autofocus—A robust tool for high resolution SAR phase correction, *IEEE Trans. Aerosp. Electron. Syst.*, *30*, 827–835.

Watters, T. R., C. J. Leuschen, J. J. Plaut, G. Picardi, A. Safaeinili, S. M. Clifford, W. M. Farrell, A. B. Ivanov, R. J. Phillips, and E. R. Stofan (2006), MARSIS radar sounder evidence of buried basins in the northern lowlands of Mars, *Nature*, *444*, 905–908.

White, O. L., A. Safaeinili, J. J. Plaut, E. R. Stofan, S. M. Clifford, W. M. Farrell, E. Heggy, and G. Picardi (2009), MARSIS radar sounder observations in the vicinity of Ma'adim Vallis, Mars, *Icarus*, *201*, 460–473, doi:10.1016/j.icarus.2009.01.015.

Withers, P. (2009), A review of observed variability in the dayside ionosphere of Mars, *Adv. Space Res.*, *44*, 277–307, doi:10.1016/j.asr.2009.04.027.

Withers, P., et al. (2012), A clear view of the multifaceted dayside ionosphere of Mars, *Geophys. Res. Lett.*, *39*, L18202, doi:10.1029/2012GL053193.

Zhang, Z., E. Nielsen, J. J. Plaut, R. Orosei, and G. Picardi (2009), Ionospheric corrections of MARSIS subsurface sounding signals with filters including collision frequency, *Planet. Space Sci.*, *57*, 393–403, doi:10.1016/j.pss.2008.11.016.